CAMBRIDGE UNIVERSITY PRESS

Machine learning algorithm to extract properties of ATE phantoms from microwave measurements

Viktor Mattsson [iD], Mauricio D. Perez, Laya Joseph and Robin Augustine

Division of Solid-State Electronics, Department of Electrical Engineering, Uppsala University, Uppsala, Sweden

Abstract

The Muscle Analyzer System (MAS) project wants to create a standalone microwave device that can assess the muscle quality, called the MAS device. To achieve that an algorithm that can derive the properties of skin, fat and muscle from the measurements is needed. This paper presents a machine learning algorithm that aims to do precisely that. The algorithm relies on first predicting the skin using the data from the MAS device, then predicting the fat again using the data from the MAS but also the predicted skin value and lastly the muscle is predicted using the microwave data together with the skin and fat predictions. Data have been collected in phantom experiments, materials that mimic the dielectric properties of human tissues. The algorithm is trained to predict the properties of said phantoms. The results show that the prediction for skin thickness works well, the fat thickness prediction is okay but the muscle prediction struggles. This is partly due to the error from the skin and fat layers are propagated to the muscle layer and partly because the muscle layer is farthest away from the sensor, which makes getting information from that layer harder.

Introduction

Poor muscle quality is a problem that can have adverse affects, it impairs one ability to perform daily tasks, decreases quality of life and leads to higher health care costs [1]. Today, the gold standard to quantify the muscle quality is via the skeletal muscle index (SMI) [2]. SMI is derived from a CT-scan done at the third lumbar level, it is an accurate method but also costly and not always available. Other techniques exist as well, like handgrip strength, which can be used as a screening tool to test strength and performance that has an indirect relation muscle mass. Bio-impedance analysis and ultrasound are two other alternative techniques that are widely available but they can suffer from interobserver variability [3]. Therefore a need for alternative methods have been identified [1, 2]. The Muscle Analyzer System (MAS) is a European project that wants to assess the muscle quality by predicting the body tissue composition. A standalone device is currently being investigated in its feasibility to do this.

To create a microwave device capable of assessing tissue properties some form of algorithm to analyze the data is needed. With the help of machine learning models can be learned from the sensor data to predict the properties. Microwave sensing enabled by machine learning has been used in several areas, to find contaminants in the food industry [4], to help with breast cancer detection [5] and to mitigate the effect of temperature on microwave sensors [6]. Another modality in terms of microwave sensing is microwave radiometry (MWR). It detects changes in temperature, and has been used to diagnose and monitor inflammatory arthritis [7], measure brain temperature [8] and to aid in breast cancer diagnosis with the help of deep learning [9]. The key difference between the microwave sensing in this work and MWR is that MWR detects thermal anomalies whereas in this approach the focus is on assessing the tissue properties not finding anomalies from an expected state.

Collecting data from patients or volunteers can be a time consuming endeavor. Therefore doing measurements on manufactured materials, called phantoms, that mimic the properties of real human tissue can be used as a proof-of-concept. Phantoms have been used to help develop devices for breast cancer detection [10, 11] and brain imaging [12]. In this paper phantoms are used to evaluate the presented machine learning algorithm.

The initial work in the MAS project covered a clinical campaign where a split-ring resonator was used as the sensor for the MAS device in a clinical campaign looking for correlations to the SMI. After concerns of its penetration depth new alternative sensors were evaluated via simulations [13]. One of those alternative was the bandstop sensor, the sensor currently used. It was manufactured and used in a small clinical campaign where the change in resonance was correlated to ultrasound measurements [14].

To aid in the analysis of muscle quality this paper presents a novel algorithm that predicts the properties of skin, fat and muscle phantoms, more precisely the thickness of the skin and fat phantoms and relative permittivity of muscle phantoms. The following sections explain the MAS device, the data collected in the phantom experiments and the idea behind the proposed algorithm in detail. The results of the algorithm on the data from the phantom experiments are then presented followed by a discussion section reflecting on the results and the algorithm. The paper is closed with some concluding remarks and ideas for the future.

The MAS project

Sensing principle

The principal idea of MAS relies on that the frequency response from the sensor varies when the dielectric properties of the Area Under Test (AUT) changes. For our case the properties change in two primary ways between measurements. First, the tissue composition change in the AUT, i.e. the skin and fat thickness varies. Secondly, poor muscle quality can be characterized by fat infiltration into the muscle tissue [15]. At microwave frequencies there is a high contrast between the relative permittivity of fat and muscle. At 2.45 GHz fat has $\varepsilon_r = 5.2$ and muscle has $\varepsilon_r = 52.7$ [16], meaning the dielectric properties of the AUT will differ if there is fat infiltration into the muscle. This contrast can be exploited to assess muscle quality.

MAS device

The MAS device comprises a sensor, Vector Network Analyzer (VNA) and a laptop. In the phantom experiments a Keysight N9918A was the VNA used. In previous works of the MAS project a different VNA was used, that was smaller, which made the overall device more portable, but it was not as accurate as the Keysight N9918A. Figure 1 shows the setup of the experiment where the Keysight VNA is connected to a laptop running a Jupyter Notebook that controls the VNA. The notebook sets the correct settings and runs and stores the measurements, making the process of conducting the measurements more organized and faster. The measurements are done from 1 to 10 GHz with a resolution of 1 MHz.

The sensor used in the measurements is a bandstop filter. Figure 2(a) is a photograph of the sensor with a superstrate layer. Figure 2(b) shows a schematic of the bandstop structure on the substrate layer under the superstrate. The sensor is based on a microstrip interdigital resonator which incorporates multiple resonators. Therefore the sensor exhibits multiple resonances/stopbands in the 1–10 GHz that repeats at their respective harmonic frequencies. At higher frequencies the different components of the bandstop structure interfere with each other accentuating a very low coupling between the two ports. It has been evaluated via simulations, where it was able to show a difference in its resonance frequency between normal muscle tissue, $\varepsilon_r = 52$ at 2.45 GHz, and muscle tissue with a high fat infiltration, $\varepsilon_r = 12$ at 2.45 GHz, for fat thicknesses of up to 10 mm [13]. The bandstop sensor has also been used in a clinical campaign, involving only a few patients. In that campaign comparative ultrasound measurements were made measuring the cross-sectional area of the rectus femoris muscle. One patient had multiple measurements during a prolonged hospital stay. For that patient the MAS device showed an inverse correlation between the resonance frequency of the sensor and ultrasound
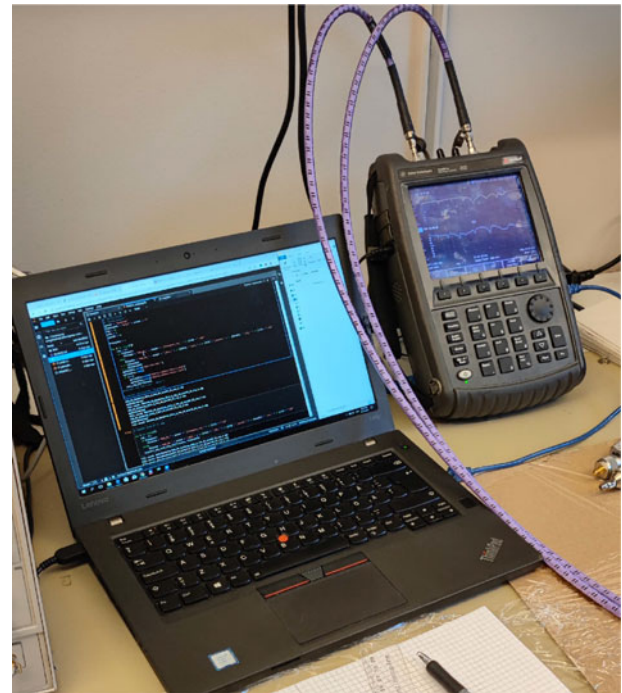

Figure 1. Setup of MAS device in the phantom experiments.

measurements of the muscle, the resonance frequency increased as the area of the muscle decreased over time [14].

Phantom experiments

ATE (Artificial Tissue Emulating) phantoms are manufactured material with the purpose of mimicking properties of real human tissues. In the context of this work the phantoms are made to mimick their dielectric properties. The phantoms were created based on Joseph [17]. Three types of phantoms were manufactured for the phantom experiments: skin, fat and muscle. To reliably create phantoms with the desired size, molds that the phantoms could be poured into were designed and 3D-printed. Figure 3 shows the manufactured fat and muscle phantoms in these molds, covered in plastic wrap. Each phantom is 15 by 10 cm in length and width with varying thickness. Table 1 lists all the different phantoms. Skin has three different thicknesses, 1.5, 2 and 2.5 mm which roughly covers the range of skin thickness in the anterior thigh reported in literature [18, 19]. For the fat phantom five different thicknesses were made. It has been reported that in the anterior thigh the average thickness of the subcutaneous fat layer is about 8 mm with a standard deviation of 6 mm, therefore thicknesses 2, 8 and 14 mm were chosen to cover this range [19]. From the previously published simulation results using the bandstop sensor [13], 10 mm were about the maximum thicknesses the fat layer could be before no difference between normal muscle and fat infiltrated muscle could be detected. Therefore a 10 mm fat phantom was made as well. The thickness of 30 mm was chosen to cover the case of a very thick fat layer. The reason for mimicking the tissue composition of the thigh is that thigh is a good indicator of whole body muscle mass [20], meaning it is an ideal position for measurements on volunteers and patients using the MAS device.
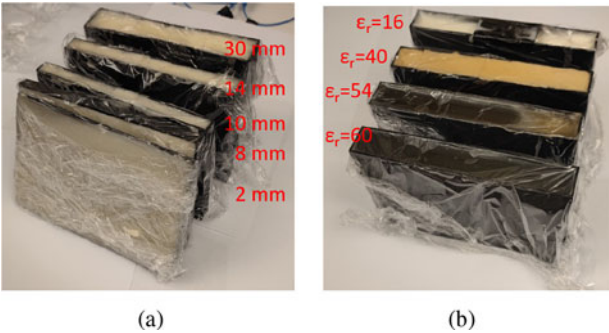
All muscle phantoms had a thickness of 20 mm. To emulate different levels of fat infiltration into the muscle tissue the relative

(a)

(b)
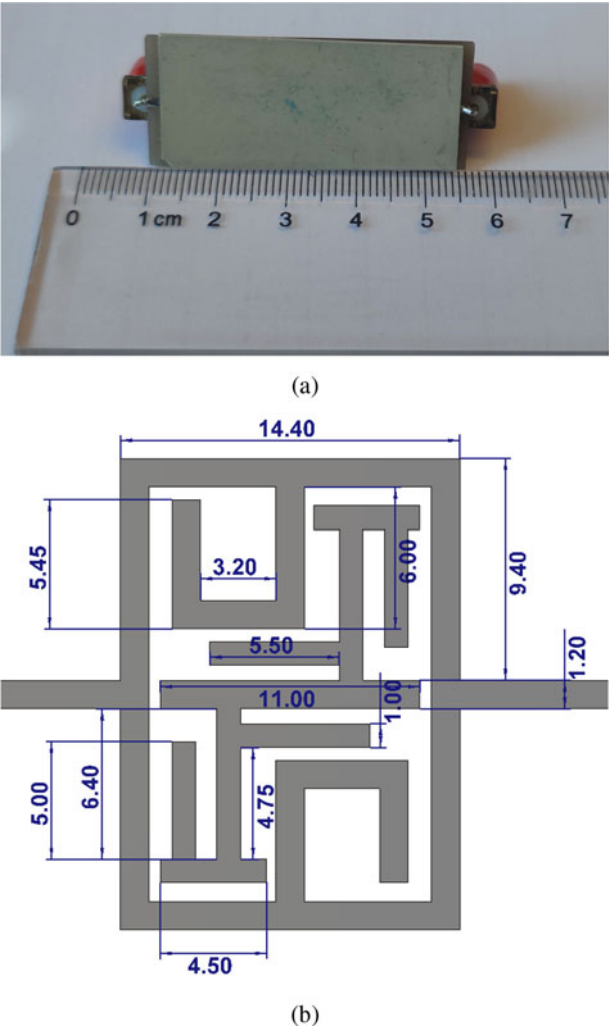
Figure 2. (a) Photo of bandstop sensor. (b) Schematic drawing of the bandstop structure underneath the superstrate, dimensions given in mm [14].

Figure 3. The fat (a) and muscle (b) phantoms in their 3D printed molds.

Table 1. Table of thicknesses and values of phantoms

Phantom	Thickness (mm)	ε_r@2.45 GHz
Skin	1.5, 2, and 2.5	38
Fat	2, 8, 10, 14, and 30	5
Muscle	20	16, 40, 54, and 60

Figure 4. Measurement on three-layer phantoms.

permittivity of the phantom was altered. Decrease in healthy muscle dielectric property represents fat infiltration in muscle. Fat infiltrated muscle is realized by iteratively varying reagent ratios described in [17]. Table 1 lists the muscle phantoms, where the value $\varepsilon_r = 54$ is the closest to the value found in literature ($\varepsilon_r = 52.7$). Originally, the muscle phantoms were meant to have ε_r of 15, 30, 40 and 52 in order to have normal muscle tissue and three levels of fat infiltration where ε_r of 15 would be the highest amount of fat infiltration. After characterizing the manufactured phantoms with a Keysight N1501A dielectric probe of ε_r the values were higher than expected for the three of the four phantoms. Therefore the values listed in Table 1 varies slightly. For the purposes of these experiments the discrepancy does not matter because the phantom with $\varepsilon_r = 54$ is close to the value found in literature, $\varepsilon_r = 52.7$, and the purpose is to be able to detect different values of ε_r.
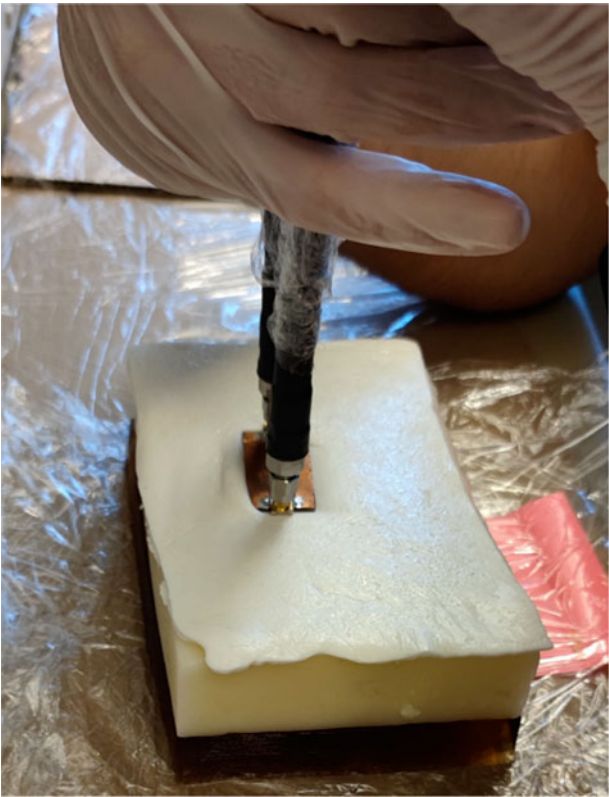
The phantom experiments were performed in December 2021. In total there are 60 unique combinations of skin, fat and muscle phantoms, 3 skin phantoms × 5 fat phantoms × 4 muscle phantoms = 60 combinations. Each combination is measured three times to ensure a good repeatability between measurements and potential outliers could be identified and removed.

Figure 4 show the phantoms during a measurement with the bandstop sensor. The phantoms are stacked with the muscle at the bottom, then fat and at the top the skin phantom. All measurements were done in approximately the center of the skin phantom.

From each measurement the resonances are derived from the minima in the amplitude. Figure 5 shows an example of one of the measurements where the blue line shows the amplitude, corresponding to the left y-axis, and the diamonds indicate the identified resonances. The dashed red line shows the unwrapped phase,
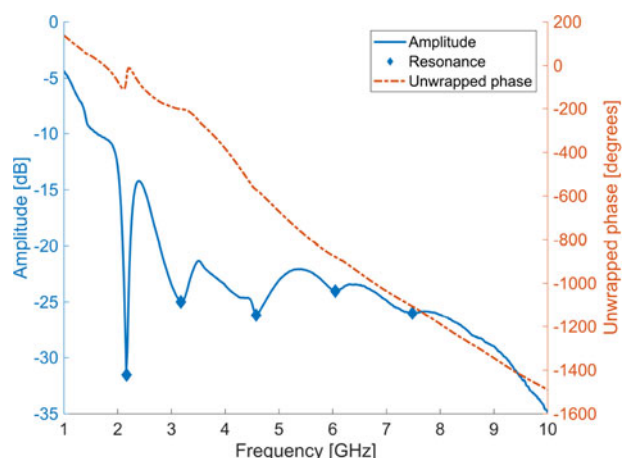
Figure 5. The amplitude and unwrapped phase from one of the measurements. The blue diamonds highlight the identified resonances.

corresponding to the right *y*-axis. As seen in Fig. 5 several minima are present, this is due to the sensor design as explained in "MAS Device" section. The number of resonances identified varied between measurements from a minimum of three to a maximum of five. In the measurement shown in Fig. 5 five points were identified. From each resonance three parameters are derived,

(1) the frequency of the resonance,
(2) the amplitude at the resonance frequency, and
(3) the quality factor of 3 dB, $Q_3 = f_r / \Delta f_{3dB}$.

Moreover the phase of the measurement is unwrapped and the slope of the unwrapped phase from 1 to 3 GHz is calculated and added as an additional parameter. In the range 1–3 GHz the first resonance is encapsulated, the slope could be calculated for a frequency range around each of the identified resonances but as seen in Fig. 5 the slope is similar across the whole frequency spectrum. However, since the value of the slopes would be similar, doing so would cause redundant information being used as input in the algorithm. Therefore, only the calculated slope from 1 to 3 GHz is considered. In total a maximum of 16, 5 resonances × 3 parameters + slope of unwrapped phase, parameters are derived from each measurement, called the MAS parameters.

Three-stage algorithm

The skin and fat layers are between the muscle phantom and sensor, i.e. for the signal to reach from the sensor to the muscle it must penetrate the skin and fat. In order to be able to accurately assess

the muscle quality good knowledge of the skin and fat thickness is crucial, whether it is data from phantom experiments or patient measurements. Therefore in order for the MAS device to be able to assess the muscle quality it also needs to accurately estimate the skin and fat layers.

To achieve this we propose the "three-stage algorithm," illustrated in Fig. 6. Its purpose is to be a method to assess all three tissue layers, skin, fat and muscle. Its key characteristic is that the prediction of the previous layers is fed forward and used in the prediction of the subsequent layers, i.e. skin is used in the prediction of fat and muscle and the fat is used in the prediction of the muscle. The algorithm can be broken into three stages, hence the name. In the first stage the skin thickness is predicted using the MAS parameters, the parameters derived from the resonances and slope of the phase for each measurement, as input and the skin data is used as the ground truth to train a machine learning model. In the second stage, the fat is predicted in a similar way, although in this case the skin prediction is included as input to the model together with the MAS parameters and in the third stage the skin and fat prediction is used, together with the MAS parameters, to predict the muscle.

There are a few discrete values for each type of phantom, therefore predicting the phantom properties is a classification problem rather than a regression problem. Each "tissue" prediction box in Fig. 6 consist first of a standard *z*-score normalization of the MAS parameters, and tissue values, if any. Any missing values are replaced with the numerical value 2. In the case of *z*-score normalization the values are adjusted to have mean 0 and standard deviation 1 on a Gaussian distribution, meaning the value 2 are two standard deviations above the mean. Secondly, the prediction boxes consist of a machine learning classifier. To find the most optimal models an exhaustive gridsearch is performed including multiple models and their respective hyperparameters. The models are trained using MAS parameters derived from the S_{21} and S_{12} parameters from the measurements, where 80% of the data is used for training and 20% for testing. The accuracy score is used as the metric to evaluate its performance. The algorithm is implemented in Python using the Scikit-Learn package [21].

Feature selection

Using all MAS parameters, also referred to as features, at every stage of the three-stage algorithm is most likely not the ideal strategy. For example, in Fig. 5 the amplitude of the first resonance is −31.5 dB, if this were the same across all measurements the parameter would provide no insight into the phantom composition and should therefore be discarded for use in the classifier models. Furthermore, different features can detect different changes in the phantom composition. One feature might be more sensitive to changes of the skin thickness while another might be more
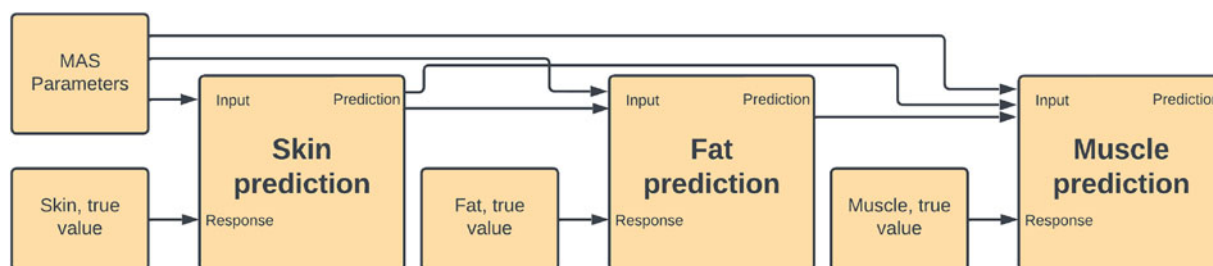
**Figure 6.** The three-stage algorithm.
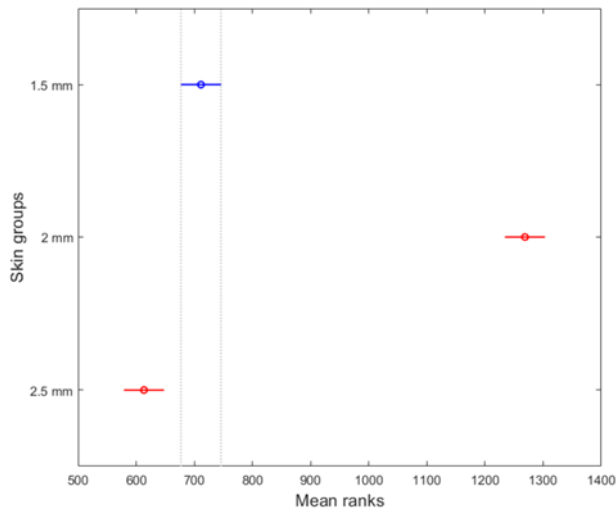
Figure 7. Visualization of how good parameter combinations were identified using the Tukey–Kramer test.

Figure 8. Flowchart of the splitting classification of the (a) fat and (b) muscle data.

attuned to changes in the fat thickness. Therefore it is crucial to select the most important features to use at every stage of the algorithm. To achieve that an exhaustive search for the best parameter combination was implemented in Matlab, where all 65,535 ($2^{16} - 1$) parameter combinations were evaluated. The method uses the Kruskal–Wallis test together with the Tukey–Kramer test to achieve this. The Kruskal–Wallis test identifies viable parameter combinations based on the p-value. This essentially tells if there exist any differences between two or multiple groups but not between which groups. Parameter combinations that fail the Kruskal–Wallis test can be discarded. After that the Tukey–Kramer test comes in. It can identify which groups are deemed statistically significantly different from other groups and which are not. Figure 7 show a visualization of the result from the Tukey–Kramer test on a set of parameters where the test manages to separate the three skin groups from each other. In the visualization the horizontal lines represent a confidence interval for each group. Groups that do not have overlapping lines are statistically significant different from each other according to the test. Good parameter combinations can be identified by finding the combinations where no groups are overlapping.

Splitting approach

Some of the phantom values are close to each other, for fat the values 8 and 10 mm and for muscle the three largest values in terms of ε_r (40, 54 and 60, from Table 1) are all closer than the phantom with $\varepsilon_r = 16$ is to the phantom with $\varepsilon_r = 40$. To accurately predict the classes where the values are far apart and close at the same time can be difficult for one model and a set of features. Therefore, the splitting approach is proposed. Figure 8 shows how the fat and muscle data can be split into two different steps, in each "Step" a different machine learning model using different features is trained. For fat, the phantoms with 8 and 10 mm is treated as the same group in the first step, so one model is trained to separate the three groups, 2 mm, 8 + 10 mm and 14 mm, in step 1 and then in the second step another model is trained to separate 8 mm from 10 mm. In similar fashion the muscle prediction is broken into two steps, first separating the phantoms with ε_r of 40–60 from $\varepsilon_r = 16$ and then in the second step ε_r values 40–60 are separated from each other.
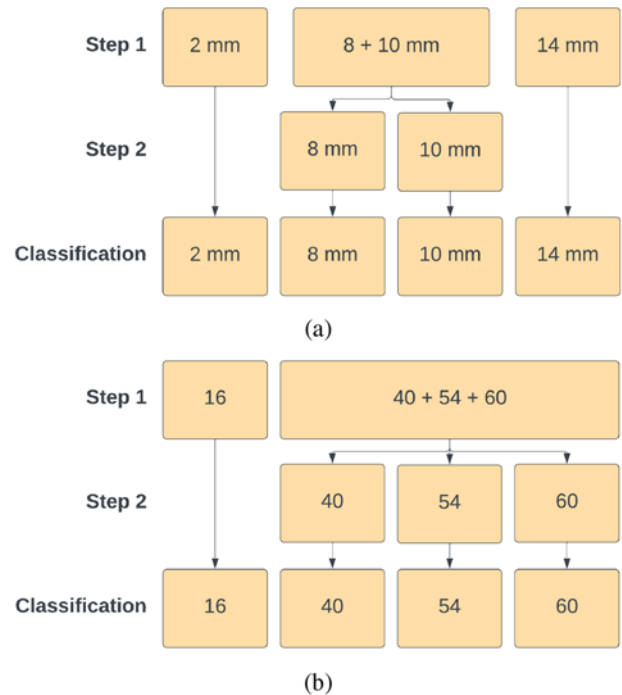
The main motivation behind the splitting approach is that different features can extract different trends in the data. Figure 9 visualizes this. In Fig. 9(a), step 1, where the fat data of 8 and 10 mm have been combined into one group a subset of features were identified where, according to the Tukey–Kramer test, all groups are deemed statistically significantly different from one another. Similarly in step 2, Fig. 9(b) a different subset of features deem the 8 and 10 mm fat data statistically significantly different. By training one classifier, using the identified features, for step 1, then feeding the "8 + 10 mm" group forward to step 2, where a different classifier, using a different subset of features, is trained, the overall fat prediction can become more accurate. The same principle applies for the muscle splitting approach.

Results

From the gridsearch different machine learning models were identified for the different stages of the algorithm, the exact models are listed in Table 2. The hyperparameters are only listed if they differ from the default value in Scikit-Learn v.1.1.3. The classifier SVM means support vector machine and the kernel RBF is radial basis function.

Figure 10 shows the confusion matrices for the skin, fat and muscle prediction when predicting on the test set. Based on the simulation analysis in Mattsson et al. [13] the theorized maximum thickness of the fat layer was 10 mm, at thicknesses above this the bandstop sensor was unable to detect difference between normal muscle tissue and muscle tissue with high fat infiltration. Therefore, the measurements with 30 mm fat phantom were excluded from the analysis since this is well above the 10 mm threshold. A large error in its prediction would impact the results of the muscle classification as the results of the fat classification get fed forward in the algorithm. Therefore there are only four fat groups. The number shown is a proportion of the true label, meaning the numbers in the
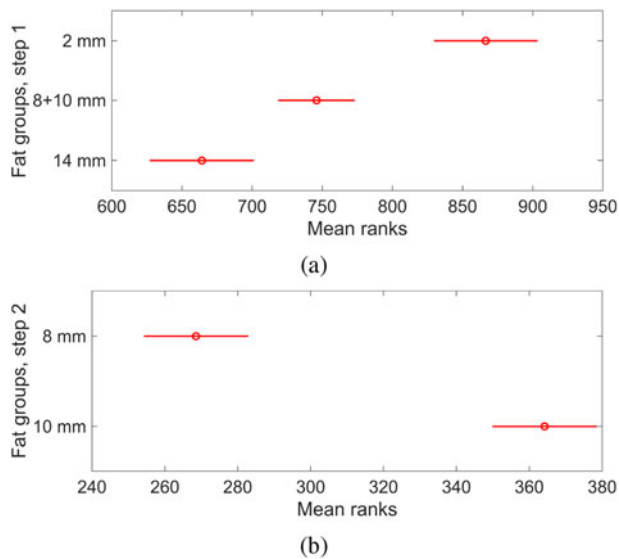
Figure 9. Tukey–Kramer test visualization of good parameter combinations for (a) step 1 and (b) step 2 for the fat splitting approach.

Table 2. Details of models used in the three-stage algorithm

Phantom	Classifier	Kernel	Hyperparameters
Skin	RandomForest	NA	$n = 1000$, depth $= 5$, samples $= 0.5$
Fat, no splitting	SVM	Linear	$C = 1000$
Fat, splitting, step 1	SVM	Poly	$C = 1000$, shape $=$ ovo
Fat, splitting, step 2	RandomForest	NA	$n = 1000$, depth $= 3$, samples $= 0.5$
Muscle, no splitting	SVM	RBF	$C = 1000$, shape $=$ ovo
Muscle, splitting, step 1	SVM	RBF	$C = 1000$, shape $=$ ovo
Muscle, splitting, step 2	SVM	RBF	$C = 1000$, shape $=$ ovo

NA = not applicable.

Figure 10. Confusion matrices of the (a) skin, (b) fat, and (c) muscle classification on the test set.
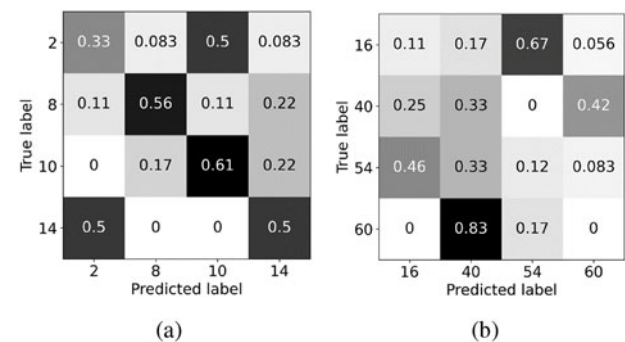
Figure 11. Confusion matrices of the (a) fat and (b) muscle classification on the test set when implementing the splitting approach.
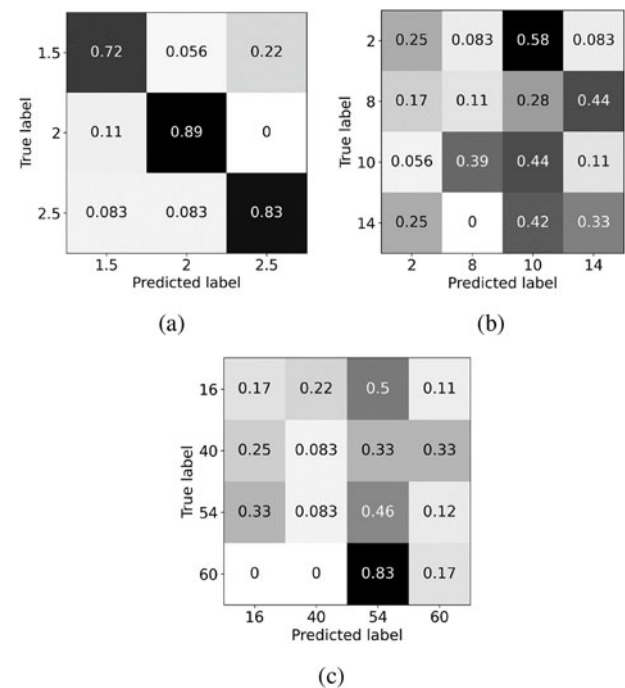
matrix rows add up to 1. After removing the fat with 30 mm there are 48 phantom combinations left in the dataset. 38 are used for training and 10 for testing, $38/48 = 79.2\%$ and $10/48 = 20.9\%$. From each set of phantoms six datasets are used, 3 repetitions and 2 S-parameters. This leads to 228 datasets in the training set and 60 in the test set. Special care is taken to avoid datasets from the same phantom set being in both the training and test set.

The confusion matrices in Fig. 11 show the results of the fat and muscle classification when implementing the splitting approach. For the skin prediction no splitting was necessary so its results is the same as in the "non-splitting" approach.

Table 3 lists the accuracy score when predicting on the train and test set for the confusion matrices shown in Fig. 10 and 11.

Discussion

The results show that the skin prediction is accurate with a score of 0.82 on the test set. The cases where there is a misprediction

Table 3. Accuracy score of each phantom type, splitting and non-splitting

Phantom	Train score	Test score
Skin	0.96	0.82
Fat, no splitting	0.82	0.28
Fat, splitting	0.72	0.52
Muscle, no splitting	0.89	0.27
Muscle, splitting	0.39	0.15

are pretty evenly spread out, as seen in Fig. 10(a). The fat prediction when not splitting is not accurate. The most accurate is the prediction of 10 mm fat, but that could also be because the model predicts 10 mm in a lot of cases. However, when applying the splitting approach, the results improve substantially as seen in Fig. 11(a) and by the test scores in Table 3. Ideally, the prediction of 2 mm should be more accurate since it is the thinnest layer and the signal should more easily penetrate the thin fat phantom. One reason

could be that the boundaries of the fat phantoms create some interference on the signal and since the 2 mm fat phantom is so thin it is more affected than the others. Considering the upper bound in terms of fat thickness for the bandstop sensor to detect difference in the muscle was 10 mm, as theorized in [13], the 0.5 accuracy for fat of 14 mm is a good result. The prediction on the muscle phantoms is less accurate, in both the non-splitting and splitting approach, when compared to the skin and fat splitting results. This is most likely due to two primary reasons. One being that the misprediction happening in the skin and, to a larger extent, the fat layer is fed-forward to the muscle prediction confusing the model. This also an issue in the fat prediction but less so since the skin prediction is quite accurate. The other reason is simply that the muscle layer is the one farthest away from the sensor, the full signal will not reach the muscle layer, some of it will get reflected in the boundaries of the skin and fat layers. Therefore, the overall frequency response of the sensor will contain less information from the muscle layer and will be more influenced by the skin and fat layers.

In the context of the phantom experiments when the tissue values we deal with are a few known discrete values the splitting approach is an interesting idea and works well for the classification of the fat data. In patient or volunteer measurements where the ground truth label would be acquired via ultrasound for example, we have continuous values rather than discrete, turning our classification problem into a regression problem. Utilizing the splitting approach in that context is not as obvious but it can be altered to use the idea. The first step could be a classifier predicting if the fat thickness is above or below the average fat thickness, or some other threshold. The next step would be two regression models, one predicting on the lower fat thickness data and the other on the higher fat thickness data. Having these two models rather than just a single one could help making the overall prediction more accurate.

The proposed algorithm is not limited to the bandstop sensor used in the phantom experiments. It could just as easily be used with any other microwave sensor.

The idea of the two-step feature selection does seem to work well. In initial tests of the algorithm features were selected on the best *F*-score determined by the ANOVA test. This works well in the binary case, when we only have two classes. But in a multiclass problem it is not obvious that feature selection strategy will work well, since the ANOVA test, similarly to the Kruskal–Wallis test, tells us if there are differences between two groups, not that all groups are different. Therefore, by using the Tukey–Kramer test as a second step the feature selection became much more computationally expensive but also more robust and subsequently the results improved. The fat results in the splitting idea are a great example of this. One set of features were identified to distinguish the three groups in step 1 (Fig. 8(a)) and another set to help separate thicknesses of 8 and 10 mm.

Conclusions

In this paper a novel algorithm that aims to predict the size, for skin and fat, and the dielectric properties of muscle is presented. Its goal is to be used in a standalone device using a microwave sensor that can assess muscle quality. The results presented here are on data acquired via measurements done on phantoms. The prediction on the skin phantom showed high accuracy, the fat results improved significantly after implementing the splitting approach. However, the muscle prediction was worse, partially due to the misprediction

getting fed forward to it and also due to it being the layer that is furthest away from the sensor.

Apart from the phantom experiments measurements with the MAS device have been performed in a volunteer study where ground truth values were obtained via ultrasound. To further validate the three-stage algorithm its performance will be evaluated on that data.

References

1. **Prado CM, Purcell SA, Alish C, Pereira SL, Deutz NE, Heyland DK, Goodpaster BH, Tappenden KA and Heymsfield SB** (2018) Implications of low muscle mass across the continuum of care: A narrative review. *Annals of Medicine* **50**(8), 675–693.
2. **Cruz-Jentoft AJ, Bahat G, Bauer J, Boirie Y, Bruyére O, Cederholm T, Cooper C, Landi F, Rolland Y, Sayer AA, Schneider SM, Sieber CC, Topinkova E, Vandewoude M, Visser M, Zamboni M, Bautmans I, Pierre Baeyens J, Cesari M, Cherubini A, Kanis J, Maggio M, Martin F, Michel JP, Pitkala K, Reginster JY, Rizzoli R, Sánchez-Rodríguez D and Schols J** (2019) Sarcopenia: Revised European consensus on definition and diagnosis. *Age and Ageing* **48**(1), 16–31.
3. **Pinto A, Pinto F, Faggian A, Rubini G, Caranci F, Macarini L, Genovese EA and Brunese L** (2013) Sources of error in emergency ultrasonography. *Critical Ultrasound Journal* **5**(S1), S1.
4. **Urbinati L, Ricci M, Turvani G, Vasquez JAT, Vipiana F and Casu MR** (2020) A machine-learning based microwave sensing approach to food contaminant detection. In *2020 IEEE International Symposium on Circuits and Systems (ISCAS)*. Seville: IEEE, 1–5.
5. **Gopal VN, Al-Turjman F, Kumar R, Anand L and Rajesh M** (2021) Feature selection and classification in breast cancer prediction using IoT and machine learning. *Measurement* **178**, 109442.
6. **Kazemi N, Abdolrazzaghi M and Musilek P** (2021) Comparative analysis of machine learning techniques for temperature compensation in microwave sensors. *IEEE Transactions on Microwave Theory and Techniques* **69**(9), 4223–4236.
7. **Laskari K, Siores E, Tektonidou M and Sfikakis P** (2023) Microwave radiometry for the diagnosis and monitoring of inflammatory arthritis. *Diagnostics* **13**(4), 609.
8. **Shevelev O, Petrova M, Smolensky A, Osmonov B, Toimatov S, Kharybina T, Karbainov S, Ovchinnikov L, Vesnin S, Tarakanov A and Goryanin I** (2022) Using medical microwave radiometry for brain temperature measurements. *Drug Discovery Today* **27**(3), 881–889.
9. **Jolen L, Galazis C, Popov L, Ovchinnikov L, Kharybina T, Vesnin S, Losev A and Goryanin I** (2022) Dynamic weight agnostic neural networks and Medical Microwave Radiometry (MWR) for breast cancer diagnostics. *Diagnostics* **12**(9), 2037.
10. **Joseph L, Asan NB, Ebrahimizadeh J, Chezhian AS, Perez MD, Voigt T and Augustine R** (2020) Non-invasive transmission based tumor detection using anthropomorphic breast phantom at 2.45 GHz. In *2020 14th European Conference on Antennas and Propagation (EuCAP)*. Copenhagen: IEEE, 1–5. https://ieeexplore.ieee.org/document/9135953/
11. **Vispa A, Sani L, Paoli M, Bigotti A, Raspa G, Ghavami N, Caschera S, Ghavami M, Duranti M and Tiberi G** (2019) UWB device for breast microwave imaging: Phantom and clinical validations. *Measurement* **146**, 582–589.
12. **Mohammed BJ and Abbosh AM** (2014) Realistic head phantom to test microwave systems for brain imaging. *Microwave and Optical Technology Letters* **56**(4), 979–982.

13. **Mattsson V, Ackermans LLGC, Mandal B, Perez MD, Vesseur MAM, Meaney P, Ten Bosch JA, Blokhuis TJ and Augustine R** (2021) MAS: Standalone microwave resonator to assess muscle quality. *Sensors* **21**(16), 5485.

14. **Mattsson V, Perez MD, Ackermans LLGC, Vesseur MAM, Bels JLM, van de Poll MCG, Mandal B, Sanchez-Gonzalez P, Seiffert AP, GomezEJ, Meaney P, Ten Bosch JA, Blokhuis TJ and Augustine R** (2022) Muscle analyzer system: Exploring correlation between novel microwave resonator and ultrasound-based tissue information in the thigh. In *2022 16th European Conference on Antennas and Propagation (EuCAP)*. Madrid: IEEE, 1–5.

15. **Baracos V and Kazemi-Bajestani SMR** (2013) Clinical outcomes related to muscle mass in humans with cancer and catabolic illnesses. *The International Journal of Biochemistry & Cell Biology* **45**(10), 2302–2308. https://linkinghub.elsevier.com/retrieve/pii/S1357272513002008

16. **Andreuccetti D, Fossi R and Petrucci C** (1997) An Internet resource for the calculation of the dielectric properties of body tissues in the frequency range 10 Hz–100 GHz. Florence: IFAC-CNR, http://niremf.ifac.cnr.it/tissprop/

17. **Joseph L** (2019) Development of ultra-wide band 500 MHz–20 GHz heterogeneous multi-layered phantom comprises of human skin, fat and muscle tissues for various microwaves based biomedical application. *Master's Thesis*. Uppsala University.

18. **Jain SM, Pandey K, Lahoti A and Rao PK** (2013) Evaluation of skin and subcutaneous tissue thickness at insulin injection sites in Indian, insulin naïve, type-2 diabetic adult population. *Indian Journal of Endocrinology and Metabolism* **17**(5), 864.

19. **Akkus O** (2012) Evaluation of skin and subcutaneous adipose tissue thickness for optimal insulin injection. *Journal of Diabetes & Metabolism* **3**(8), 1–6.

20. **Jung Lee S, Janssen I, Heymsfield SB and Ross R** (2004) Relation between whole-body and regional measures of human skeletal muscle. *The American Journal of Clinical Nutrition* **80**(5), 1215–1221.

21. **Pedregosa F, Varoquaux G, Gramfort A, Michel V, Thirion B, Grisel O, Blondel M, Prettenhofer P, Weiss R, Dubourg V, Vanderplas J, Passos A, Cournapeau D, Brucher M, Perrot M and Duchesnay E** (2011) Scikit-learn: Machine learning in Python. *Journal of Machine Learning Research* **12**, 2825–2830.

Viktor Mattsson is currently a PhD student at Uppsala University working on data analysis on microwave sensor data in clinical applications. He received M.Sc. in Engineering Physics with a specialization in Scientific Computing from Uppsala University in 2018. His research interest includes data-driven modeling in biomedical applications with the help of machine learning and applying the models it in specialized hardware, such as FPGAs.

Dr Mauricio Pérez graduated in Electronics Engineering from the National University of Technology, Argentina, in 2007. Received the Doctoral degree in Electrical Engineering from the University of Bologna, Italy, in 2012. His thesis topic was in microwave characterization of materials. He worked as Industrial Researcher for the food and fashion industries in Italy from 2012-2014 and as a Teacher and Researcher at the National University of Technology, Argentina, from 2014 to 2017. Currently, Senior Researcher at Uppsala University, Sweden, since 2018, working in Medical and Microwave Engineering. He is author and coauthor of more than 75 publications, including journals and conferences, and reviewer of several reputed engineering journals. His research interest includes modeling and data-driven validation of microwave sensors for biomedical applications and body-centric communications. He is also co-founder and Director of R&D of Probingon AB (Swedish start-up company) specialized in point-of-care sensors.

Laya Joseph received the Engineering degree in Electronics and Communication from Calicut University, India, in 2009, and the master's degree in Engineering Physics from Uppsala University, Sweden, in 2019. She is currently doing her PhD in Microwaves in Medical Engineering Group (MMG), Division of Solid-State Electronics, Department of Electrical Engineering, Angstrom Laboratoriet, Uppsala Universitet (UU), Sweden. She has worked as Research Engineer with the Micro Structure Technology (MST), Material Science Department in 2020. Also, she has worked as research engineer the Angstrom Laboratory, Solid State Electronics Division, Microwaves in Medical Engineering Group (MMG), Uppsala University, from 2019 to 2021. Her research interests include biological microwave phantoms for intrabody communication, fat intrabody communication, breast tumor sensing, and stretchable printed circuit boards for skin worn wireless networks.

Assoc. Prof. Robin Augustine graduated in Electronics Science from Mahatma Gandhi University, India in 2003. He received master's degree in Electronics with Robotics specialization from Cochin University of Science and Technology India in 2005. Received Doctoral degree in Electronics and Optic Systems from Univeristé Paris Est Marne La Vallée, France in July 2009. He is author or co-author of more than 200 publications including journals and conferences and has three patents. He is now Senior University Lecturer at Uppsala University in Medical Engineering and Docent in Microwave Technology. He has pioneered the Fat – Intra Body Communication technique Recipient of Swedish research agency, Vetenskapsrådet's (VR) project grant 2017 for his project on A Novel Modality for Osteodiagnosis. He is Co-PI of several EU projects. He is partnering in the SSF 2022 grant Body Centric Operating System – BOS. He is currently coordinating EU HORIZON 2020 FET-OPEN Science Excellence project B-CRATOS, a visionary project in man machine interface.